Hindawi
Complexity
Volume 2020, Article ID 7254503, 15 pages
https://doi.org/10.1155/2020/7254503

Research Article

A Novel Sliding Mode Control with Low-Pass Filter for Nonlinear Handling Chain System in Container Ports

Bowei Xu,[1] **Junjun Li**,[2] **Yongsheng Yang**,[1] **Huafeng Wu**,[2] **and Octavian Postolache**[3]

[1]*Institute of Logistics Science & Engineering, Shanghai Maritime University, Shanghai 201306, China*
[2]*Merchant Marine College, Shanghai Maritime University, Shanghai 201306, China*
[3]*Instituto de Telecomunicacoes, ISCTE-IUL, Av. Das Forcas Armadas, Lisbon 1049-001, Portugal*

Correspondence should be addressed to Junjun Li; jsliljj@163.com

Received 19 November 2019; Revised 11 January 2020; Accepted 17 January 2020; Published 10 February 2020

Academic Editor: Lingzhong Guo

Nonlinearities in a container port handling chain include mainly nonnegative arrive rate of container cargoes, limited container handling completion rate, and nonnegative unsatisfied freight requirement constraints. The nonlinearity influences the operation resources availability and consequently the planned container port handling strategies. Developments presented in this work are devoted to a novel design of sliding mode control with low-pass filter (SMC-LPF) to nonlinear handling chain system (HCS) in container ports. The SMC-LPF can effectively reduce unsatisfied freight requirement of the HCS and make chattering decrease significantly. To illustrate the effectiveness and accuracy of the proposed SMC-LPF, an application to a real container port in China is outlined. The performances of the SMC-LPF for the nonlinear HCS in container ports outperform those of the traditional method, particle swarm optimization algorithm, and slide mode control under simulations with a unit step signal and a sinusoidal signal with offset as the freight requirements. The contributions herein demonstrate the proposed control strategy in weakening chattering, reducing the unsatisfied freight requirements to 0 as close as possible in the HCS, maximizing the operation resilience and robustness of port and shipping supply chain against parametric perturbation, external disturbances, and fluctuant handling abilities.

1. Introduction

Over the last decades, there has been a significant growth of global container transportation due to the fast development of global trade. Container ports play a significant role in commercial trade, serving as the crucial nodes in the global port and shipping supply chain. China has become the world's largest container gathering area [1]. Seven Chinese ports have ranked in the top ten container ports in the world since 2012. The throughput of China's ports increased from a mere 2.7 million TEUs in 1993 to 251 million TEUs in 2018 [2]. The increasing amount of container volumes undoubtedly brings much pressure to port operations. Hence, the improved operational efficiency in container ports needs to accommodate this growing demand for container freight service [3].

Container port handling is a complex and dynamic system where different types of machines (such as truck, yard crane, and gantry crane) cooperate closely to complete the transport of inbound and outbound containers between quayside and stack [4]. The container port handling chain system (HCS) may be divided into five main individual operations [5]. More specifically, they are the delivery/receipt of containers, yard crane loading and unloading operations, yard truck/AGV horizontal transportation between the berth and yard, gantry crane loading and unloading operations, and container vessel berthing [6, 7]. A close container port handling chain of efficient landside and seaside operations are inevitable to reduce dwell times and improve the service level as far as possible. As it is usually not easy to expand the infrastructure of a container port, how to effectively establish an efficient container port

HCS is of great importance for container port operations management.

1.1. Literature Review. During the past decades, academies, society, and port industry have been striving for an advanced container port handling chain system (HCS) based on analytical, simulation, and control approaches in order to stay competitive [8–10]. The analytical approaches search for the optimal solution of the handling operations by addressing the mathematical formulation. For example, Crane Choe et al. aimed at scheduling for opportunistic remarshaling of containers in an automated stacking yard to minimize the delay of the current main jobs as well as the makespan of all the jobs in the horizon [11]. Li and Jia modeled the traffic scheduling problem as a mixed integer linear program (MILP) to minimize the berthing and departure delays of vessels and the number of vessels that could not berth or depart successfully [12]. Kasm and Diabat considered the Quay Crane Scheduling Problem (QCSP) with noncrossing and safety clearance constraints and proposed a two-step approach initiated by a partitioning heuristic and terminated by a Branch and Price algorithm to acquire operationally practical solutions by minimizing crane repositioning movements [13]. Hu et al. addressed the joint vehicle dispatching and storage allocation problem in automated container terminals and proposed a PSO-based greedy search method to solve it, with the goal of minimizing the vehicle operating costs [4]. However, the vast majority disregard the operation resilience problem inherent in the container port HCS when freight requirement changes.

The simulation approaches evaluate different management policies by modeling the dynamical behavior of the container port HCS. For example, in terms of agent-oriented programming, Yin et al. described a distributed agent system for dynamic port planning and scheduling [14]. Cubillos et al. presented a decision support system based on the agent technology that helped in solving the problem of berth allocation for ships within a port [15]. With respect to object-oriented programming, Lee and Cho discussed a simulation-based dynamic planning system based on real-time tracking of yard tractors, with two scheduling rules: shortest operation time and equal load distribution among yard blocks [16]. Ursavas and Zhu studied the optimal policies for the berth allocation problem, taking into consideration the uncertain nature of the vessel arrival and handling times [17]. The simulation approaches provide port authorities with enhanced information to decide on the quality and robustness of the proposed schedules, resulting in better solutions for the HCS.

The control approaches improve the performance of the container port handling chain by optimizing control decisions on the system behaviors. For example, optimal control approach [18], model predictive scheduling [19], event-driven receding horizon control [3], robust control [7], and parameter control strategies (such as deterministic, adaptive, self-adaptive, and augmented self-adaptive) [20–22]). Despite the diversity of control approaches used to enhance port productivity and efficiency, nonlinearities of the container port HCS has been largely ignored, which does not match the actual situation of container ports and limits the practical applications. However, nonlinearities play an important role in the container port HCS, which is not only directly related to the production efficiency of terminals but also restricts and influences the operation of the other partners in the port and shipping supply chain. Therefore, it is essential to consider the nonlinearities in the container port HCS.

1.2. Motivation for Work. Port authorities need to deal with a wide variety of interrelated handling problems, and the productivity and effectiveness of the port depends on their control and scheduling solution. Management strategies are therefore necessary to increase their productivity and effectiveness, and thereby enhancing the resilience of the container port HCS. Up to present, most of the literatures about the container port HCS with a focus on its linearity from the perspective of container ports, few research efforts have been devoted to the nonlinearity of the whole HCS from the standpoint of the port and shipping supply chain. Fortunately, the nonlinearities in the container port HCS gradually begin to receive increasing attention among academies, society, and port industry. Xu et al. modeled the nonlinear handling chain in the container port with control approach. In addition, the authors demonstrated a starting point in the development of a quantitative resilience decision-making framework and mitigating the negative impacts for port authorities and other players in the port and shipping supply chain [5]. However, the exiting models and solution approaches have the following limitations that might hinder practical applications: (i) their model relies on highly simplified assumptions that reducing the complexity of the problem; as a result, the accuracy of their models may vary a lot under different dynamical conditions, and (ii) since their solution method is not a practically applicable exact approach, the method may incur unsatisfied freight service requests even if the handling plans proposed by the port operators are feasible; as a result, the port operators may need to revise their plans frequently, which is undesirable in practice. Therefore, there is a need for operational control decisions to appropriately adapt the dynamically operating environments in container ports.

Consequently, our study adds to the literature by emphasizing three important nonlinearities of the HCS in container ports, which includes nonnegative arrive rate of container cargoes, limited container handling completion rate, and nonnegative unsatisfied freight requirement constraints. The main contributions of this work are as follows: (i) a new nonlinear HCS in container ports is developed, which can be used for container handling with different freight requirements; thus, it helps to improve port service levels. (ii) A sliding mode control with the low-pass filter (SMC-LPF) for the nonlinear HCS is formulated for efficiently obtaining enhanced solutions, where strategies for coping with nonlinear constraints are proposed, a sliding mode controller with LPF is designed, and exponential reaching law is employed to improve the dynamic quality of

the reaching process. (iii) The performance of the SMC-LPF for the nonlinear HCS in container ports is measured and validated by comparing with those of the traditional method, particle swarm optimization algorithm, and slide mode control under simulations on the certain HCS (the values of freight requirements are a unit step signal and a sinusoidal signal with offset, respectively) and uncertain HCS (the uncertainties are parametric perturbation, external disturbances, and fluctuant handling abilities, respectively). The main improvements of the sliding mode control method are (i) a low-pass filter is added to weaken chattering of sliding mode control; (ii) a stable sliding mode motion with the largest sliding mode area is designed; (iii) the upper and lower limits of control signal are well constructed to deal with the nonlinear segments; (iv) the original arate, which reflects the handling requirements, is employed in the design of control signal.

2. Nonlinear Handling Chain System in Container Ports

2.1. Linear Model. The linear model of the handling chain system in container ports is shown in Figure 1. For detailed description of the handling chain system in container ports, we refer the readers to Xu et al. [5], where quay cranes, trucks, and yard cranes etc., collaborate to handle containers from the berth to yard and vice versa. However, tuning the control parameters in the linear model for implementation to real container ports is not an easy task due to coping with the dynamics of uncertainties and disturbances.

As described in Figure 1, the UFR transfer function in relation to the input FR can be calculated as follows:

$$\frac{\mathrm{UFR}}{\mathrm{FR}} = \frac{(T_G + T_I + T_I T_G s)(1 + T_F s) - T_Q - T_I}{T_I T_G T_F \left[(1/T_U T_G) + ((1/T_I) + (1/T_G))s + s^2\right](s + (1/T_F))}. \tag{1}$$

If $\mathrm{fr}(t)$ is a unit step signal, $\mathrm{ufr}(\infty)$ (final value of $\mathrm{ufr}(t)$) can be obtained by final value theorem:

$$\begin{aligned}
&\mathrm{ufr}(\infty) \\
&= \lim_{s \longrightarrow 0} s \cdot \mathrm{UFR}(s) \\
&= \lim_{s \longrightarrow 0} \frac{(T_G + T_I + T_I T_G s)(1 + T_F s) - T_Q - T_I}{T_I T_G T_F \left[(1/T_U T_G) + ((1/T_I) + (1/T_G))s + s^2\right](s + (1/T_F))} \\
&= \frac{T_U(T_G - T_Q)}{T_I}.
\end{aligned} \tag{2}$$

It can be seen that $\mathrm{ufr}(\infty)$ is equal to 0 only when $T_G = T_Q$.

2.2. Nonlinear Model. Our nonlinear model extends the nonlinear model of Xu et al. in that our model explicitly considers the unsatisfied freight requirement constraint, whereas the model of Xu et al. assumed that the value of the unsatisfied freight requirement may be negative, although it does not exist in the actual operation [5]. Under real environments of container ports, the value of $\mathrm{arate}(t)$ cannot be negative, although mathematically it holds; the upper value of $\mathrm{comrate}(t)$ is limited; $\mathrm{fr}(t)$ is not constant; $\mathrm{ufr}(t)$ should not be negative even in the case of a sharp drop in $\mathrm{fr}(t)$. However, the linear model in Figure 1 cannot guarantee these three nonlinear natures. To reflect them, a novel nonlinear handling chain system (HCS) model consisting of three nonlinear segments is given in Figure 2. There are three nonlinear segments in this model: the value of $\mathrm{arate}(t)$ cannot be less than 0, there is an upper limit value $\mathrm{COMRATE}_m$ for $\mathrm{comrate}(t)$ because of the actual limited handling ability, and the value of $\mathrm{ufr}(t)$ cannot be less than 0, where, $\mathrm{COMRATE}_m$ should not be less than $\mathrm{fr}(t)$ all the time, otherwise $\mathrm{ufr}(t)$ will continuously increase, it would congest the HCS.

Compared to the linear model (Figure 1), the nonlinear system has three more nonlinear segments. It is more complex and difficult to control $\mathrm{ufr}(t)$ in the nonlinear system for enhancing the service level and operation performance.

3. Sliding Mode Control with Low-Pass Filter for Nonlinear Handling Chain Model

A motivation to use the sliding mode control (SMC) is that it has many essential advantages such as fast response, insensitivity to parameters and disturbance changes, and simple implementation. It has been widely applied to many kinds of the nonlinear control system [23, 24]. However, there is a drawback of chattering in traditional SMC, which directly influences the performance of the controlled system. To reduce chattering in SMC and improve the control efficiency, a novel SMC-LPF in Figure 3 is designed for the nonlinear HCS in container ports. The dashed box contains two parts: the SMC and the LPF, which together form the SMC-LPF system. Similar to the nonlinear system, in Figure 2, the input signals of the sliding mode controller include $\mathrm{avfr}(t)$, $\mathrm{ufr}(t)/T_U$, and $\mathrm{efrip}(t)/T_I$. $\mathrm{arate}(t)$, the output control signal of the SMC-LPF is set as the new input to the lead policy of handling operation $1/(1 + T_G s)$.

3.1. Strategies for Coping with Nonlinear Constraints. Considering the nonlinear segments, the nonnegative $\mathrm{arate}(t)$ and the limited $\mathrm{comrate}(t)$, it is set that

$$0 \le u(t) \le \mathrm{COMRATE}_m. \tag{3}$$

The value of $u(t)$ is exponentially smoothed by a first-order lag to be $\mathrm{arate}(t)$, and the value of $\mathrm{arate}(t)$ is exponentially smoothed by a first-order lag to be $\mathrm{comrate}(t)$. When the initial values of $\mathrm{arate}(t)$ and $\mathrm{comrate}(t)$ are both in $[0, \mathrm{COMRATE}_m]$, it can be ensured that $\mathrm{arate}(t) \ge 0$ and $\mathrm{comrate}(t) \le \mathrm{COMRATE}_m$. And the fixed upper limit of $u(t)$ is also more in line with the actual handling volume because the shoreline resources of container terminals are finite and the increase of $\mathrm{comrate}(t)$ is limited.

In addition, $\mathrm{ufr}_1(t)$ instead of $\mathrm{ufr}(t)$ is managed by the SMC-LPF. The control objective is to make $\mathrm{ufr}_1(t)$ reach 0 as

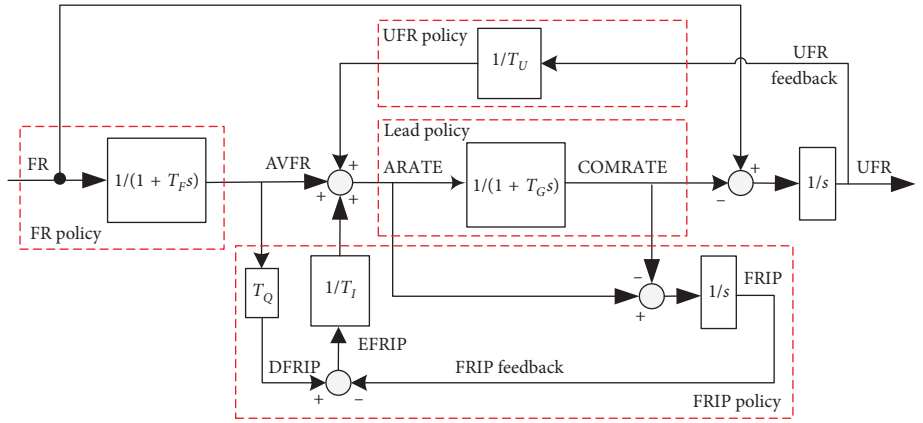

Figure 1: Linear model of handling chain system in container ports.

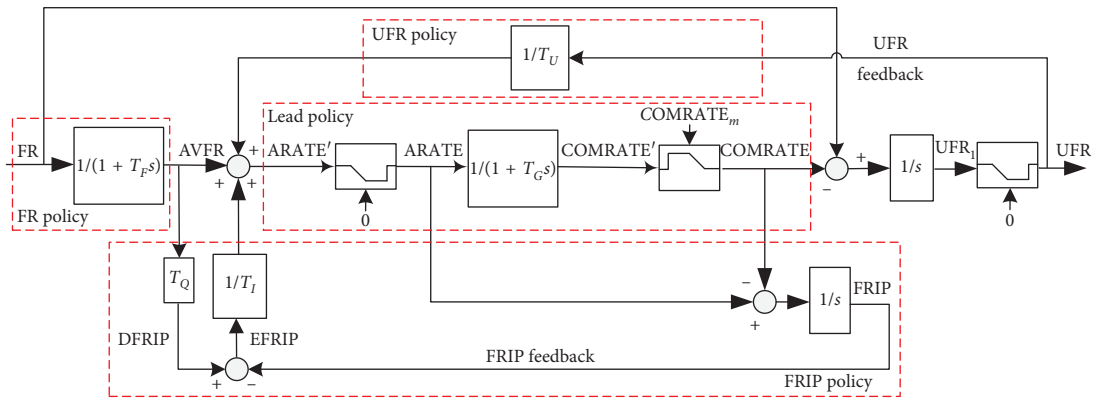

Figure 2: Nonlinear model of handling chain system in container ports.

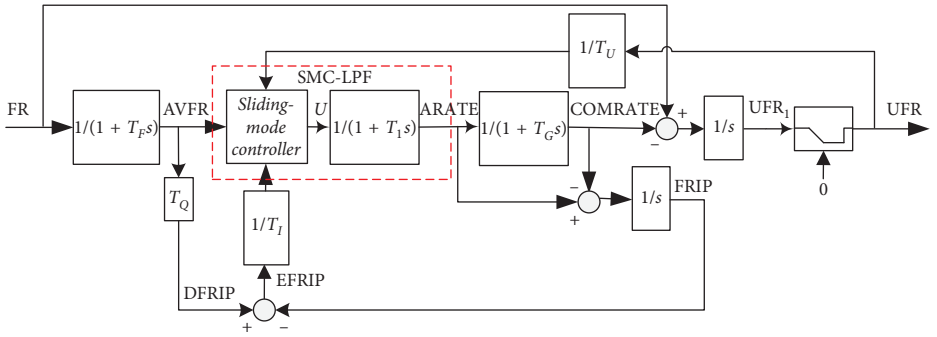

Figure 3: SMC-LPF for nonlinear HCS in container ports.

closely as possible. Then, $\mathrm{ufr}(t)$ would also be as close as possible to 0.

In summary, it can be seen that all these three constraints have been well coped with the above strategies.

3.2. Sliding Mode Controller with LPF

3.2.1. Switching Function of Sliding Mode Motion. From Figure 3,

$$\frac{\mathrm{FR}(s) - U(s)/\left[(1 + T_G s)(1 + T_1 s)\right]}{s} = \mathrm{UFR}_1(s). \tag{4}$$

Then,

$$\begin{aligned}&\left[1 + (T_1 + T_G)s + T_1 T_G s^2\right]\mathrm{FR}(s) - U(s)\\ &\quad = s\left[1 + (T_1 + T_G)s + T_1 T_G s^2\right]\mathrm{UFR}_1(s).\end{aligned} \tag{5}$$

It is set that $X_1(s) = \mathrm{UFR}_1(s)$ and $x_1(t) = \mathrm{ufr}_1(t)$. To describe simply, "$(t)$" is omitted in the following text. Then,

$$\mathrm{fr} + (T_1 + T_G)\frac{\mathrm{dfr}}{\mathrm{d}t} + T_1 T_G \frac{\mathrm{d}^2 \mathrm{fr}}{\mathrm{d}t^2} - u = \frac{\mathrm{d}x_1}{\mathrm{d}t} + (T_1 + T_G)\frac{\mathrm{d}^2 x_2}{\mathrm{d}t^2} + T_1 T_G \frac{\mathrm{d}^3 x_2}{\mathrm{d}t^3}. \tag{6}$$

It is set that $x_2 = \mathrm{d}x_1/\mathrm{d}t$ and $x_3 = \mathrm{d}x_2/\mathrm{d}t$, then the state equations are

$$\begin{aligned} \frac{\mathrm{d}x_1}{\mathrm{d}t} &= x_2, \\ \frac{\mathrm{d}x_2}{\mathrm{d}t} &= x_3, \\ \frac{\mathrm{d}x_3}{\mathrm{d}t} &= \frac{\left[\mathrm{fr} + (T_1 + T_G)(\mathrm{dfr}/\mathrm{d}t) + T_1 T_G\left(\mathrm{d}^2\mathrm{fr}/\mathrm{d}t^2\right) - u - x_2 - (T_1 + T_G)x_3\right]}{T_1 T_G}. \end{aligned} \tag{7}$$

The switching function is employed:

$$s = c_1 x_1 + c_2 x_2 + x_3. \tag{8}$$

The time derivative of s is

$$\begin{aligned} \frac{\mathrm{d}s}{\mathrm{d}t} &= c_1 \frac{\mathrm{d}x_1}{\mathrm{d}t} + c_2 \frac{\mathrm{d}x_2}{\mathrm{d}t} + \frac{\mathrm{d}x_3}{\mathrm{d}t} \\ &= \left(c_1 - \frac{1}{T_1 T_G}\right)x_2 + \left(c_2 - \frac{T_1 + T_G}{T_1 T_G}\right)x_3 \\ &\quad + \frac{\left[\mathrm{fr} + (T_1 + T_G)(\mathrm{dfr}/\mathrm{d}t) + T_1 T_G\left(\mathrm{d}^2\mathrm{fr}/\mathrm{d}t^2\right) - u\right]}{T_1 T_G}. \end{aligned} \tag{9}$$

Let $u = \begin{cases} u_+(\mathbf{x}), & s(\mathbf{x}) > 0 \\ u_-(\mathbf{x}), & s(\mathbf{x}) < 0 \end{cases}$, $\mathbf{x} = [x_1, x_2, x_3]^T$. It can be known that formulas (10) and (11) will definitely hold according to the generalized sliding mode condition:

$$\left(c_1 - \frac{1}{T_1 T_G}\right)x_2 + \left(c_2 - \frac{T_1 + T_G}{T_1 T_G}\right)x_3 + \frac{\left[fr + (T_1 + T_G)(\mathrm{dfr}/\mathrm{d}t) + T_1 T_G\left(\mathrm{d}^2\mathrm{fr}/\mathrm{d}t^2\right) - u_-\right]}{T_1 T_G} > 0, \tag{10}$$

$$\left(c_1 - \frac{1}{T_1 T_G}\right)x_2 + \left(c_2 - \frac{T_1 + T_G}{T_1 T_G}\right)x_3 + \frac{\left[fr + (T_1 + T_G)(\mathrm{dfr}/\mathrm{d}t) + T_1 T_G\left(\mathrm{d}^2\mathrm{fr}/\mathrm{d}t^2\right) - u_+\right]}{T_1 T_G} < 0. \tag{11}$$

To make the sliding mode area as large as possible, it is set that

$$c_1 = \frac{1}{T_1 T_G}, \tag{12}$$

$$c_2 = \frac{T_1 + T_G}{T_1 T_G}. \tag{13}$$

Due to $T_1 > 0$ and $T_G > 0$, the whole line of $s = 0$ is the sliding mode area if formulas (14) and (15) are satisfied:

$$u_- < u_s, \tag{14}$$

$$u_+ > u_s, \tag{15}$$

where $u_s = \mathrm{fr} + (T_1 + T_G)(\mathrm{dfr}/\mathrm{d}t) + T_1 T_G(\mathrm{d}^2\mathrm{fr}/\mathrm{d}t^2)$.

3.2.2. Stability Analysis of Sliding Mode Motion. From equation (8), it is known that the sliding mode equation is

$$s = c_1 x_1 + c_2 x_2 + x_3 = 0. \tag{16}$$

Then,

$$\frac{1}{T_1 T_G}x_1 + \frac{T_1 + T_G}{T_1 T_G}\frac{\mathrm{d}x_1}{\mathrm{d}t} + \frac{\mathrm{d}^2 x_1}{\mathrm{d}t^2} = 0. \tag{17}$$

The characteristic equation of equation (17) is

$$p^2 + \frac{T_1 + T_G}{T_1 T_G}p + \frac{1}{T_1 T_G} = 0. \tag{18}$$

Then,

$$\left(p + \frac{1}{T_1}\right)\left(p + \frac{1}{T_G}\right) = 0. \tag{19}$$

Due to $T_1 > 0$ and $T_G > 0$, the roots of the characteristic equation are both negative. It can be seen that the stability condition of sliding mode motion is satisfied, and the SMC-LPF for the nonlinear HCS in container ports is stable.

3.2.3. Exponential Reaching Law-Based u. u is the output control signal of the sliding mode controller and the input control signal of the low-pass filter. Exponential reaching law is employed here to improve the dynamic quality of the reaching process, and saturation function is used to replace sign function to further reduce chattering. Then,

$$\frac{\mathrm{d}s}{\mathrm{d}t} = -\varepsilon \cdot \mathrm{sat}(s) - k \cdot s, \tag{20}$$

where $\varepsilon, k > 0$, $\text{sat}(s) = \begin{cases} 1, & s > \Delta \\ k_\Delta s, & |s| \le \Delta \\ -1, & s < -\Delta \end{cases}$, Δ is a small positive real number, and $k_\Delta = 1/\Delta$.

From equations (9), (12), (13), and (20),

$$-\varepsilon \cdot \text{sat}(s) - k \cdot s = \frac{(u_s - u)}{T_1 T_G}. \tag{21}$$

It can be derived that

$$u = u_s + [\varepsilon \cdot \text{sat}(s) + k \cdot s] T_1 T_G. \tag{22}$$

It is obvious that formulas (14) and (15) are satisfied if u is always equal to equation (22). However, there are limits for u in the handling chain system of container ports: $u_{\min} \le u \le u_{\max}$ ($u_{\min}$ and $u_{\max}$ are the minimum and maximum values of u, which will be given in Section 3.4; then,

$$u = \min\{u_{\max}, \max\{u_{\min}, u_s + [\varepsilon \cdot \text{sat}(s) + k \cdot s] T_1 T_G\}. \tag{23}$$

To satisfy formulas (14) and (15) in every situation, $u_{\min}$, u_s, and $u_{\max}$ are required to meet the following formula:

$$u_{\min} < u_s < u_{\max}. \tag{24}$$

And from Section 3.1, it is concluded that $0 < u_s < \text{COMRATE}_m$.

3.2.4. Output of Sliding Mode Controller with LPF. The output of the SMC-LPF is arate. From Figure 3,

$$\frac{\text{ARATE}(s)}{U(s)} = \frac{1}{1 + T_1 s}. \tag{25}$$

For the convenience of analysis, let u_1 = arate, then

$$u_1 + T_1 \frac{\mathrm{d}u_1}{\mathrm{d}t} = u. \tag{26}$$

It can be calculated that

$$u_1 = e^{-(1/T_1)t} \left[u_1(0_+) + \frac{1}{T_1} \int_0^t u e^{(1/T_1)\tau} \mathrm{d}\tau \right], \tag{27}$$

where $u_1(0_+)$ is the initial value of u_1.

3.3. The Impact of Original Arate on u. In the above-mentioned SMC-LPF method, the original arate has not been considered. However, the original arate, which reflects the handling requirements, is very valuable information that should not be ignored. In this work, it is assumed that

$$u \le \mu \cdot \text{oarate}, \tag{28}$$

where $\mu (\mu \ge 1)$ is the coefficient of the arrive rate. From Figure 3, oarate = avfr + (ufr/T_U) + (efrip/T_I). To enhance the handling efficiency of container ports, we make some modifications in the SMC-LPF. If frip is lower than dfrip, it is expected that oarate is larger; else, if frip is more than dfrip, it is set that efrip has no influence on oarate. Then,

$$\text{oarate} = \text{avfr} + \frac{\text{ufr}}{T_U} + \frac{\max(0, \text{efrip})}{T_I}, \tag{29}$$

where efrip = dfrip − frip and dfrip = $T_Q \cdot$ avfr.

In equation (29), frip and avfr should be calculated. From Figure 2,

$$\begin{aligned} U_1(s) &= (1 + T_G s)\text{COMRATE}(s), \\ \text{COMRATE}(s) &= \text{FR}(s) - s \cdot \text{UFR}_1(s), \\ \text{FRIP}(s) &= \frac{U_1(s) - \text{COMRATE}(s)}{s}. \end{aligned} \tag{30}$$

Then,

$$\text{FRIP}(s) = T_G [\text{FR}(s) - s \cdot \text{UFR}_1(s)]. \tag{31}$$

frip(t) can be calculated through inverse Laplace transform of FRIP(s):

$$\text{frip} = T_G (fr - x_2). \tag{32}$$

The calculation of avfr depends on fr. In Section 4, avfr are given in the cases of specific fr.

3.4. Minimum and Maximum Values of u. The minimum value of u is only limited by formula (3); therefore, it is set that $u_{\min} = 0$. The maximum value of u is subject to formulas (3), (24), and (28). Among them, formula (24) maintains the basic performance of the SMC-LPF. To avoid conflicts among these formulas while maintaining the basic performance of the SMC-LPF, it is set that formula (28) is ignored when $s > 0$ & $u_s \ge \mu \cdot \text{arate}$ or $s < 0$ & $\mu \cdot \text{arate} \le 0$. The pseudocode of the maximum value of u is as follows:

```
If s > 0 & u_s ≥ μ · arate, or s < 0 & μ · arate ≤ 0
    u_max = COMRATE_m;
Else
    u_max = min(COMRATE_m, μ · arate).
End
```

4. Simulation Analysis

The handling chain system that motivated this study is typically a real container port in China. It has four container docks. Under normal operations, its annual container throughput would be around 4 million TEU. In the system under consideration, its resilience can be defined as its ability to preserve the specifications facing variable freight requirements. This work interprets the resilience into ITAE (the integral of time multiplied by the absolute error) of ufr. To validate the efficiency of the SMC-LPF for the nonlinear handling chain system in container ports, five cases are simulated and analyzed. In the first two cases, the handling chain system is certain and the values of fr are a unit step signal and a sinusoidal signal with offset, respectively. In the subsequent three cases, the handling chain system is uncertain. And the robustness of the proposed method is fully shown by case studies on parametric (T_G) perturbation, external disturbances, and fluctuant COMRATE$_m$. The performance of the SMC-LPF is verified by comparing simulation results with those of three other methods:

traditional method (TM), particle swarm optimization (PSO) algorithm, and slide mode control (SMC). In the TM and PSO, the nonlinear model of the handling chain system in container ports in Figure 2 is directly employed. To highlight the effect of the low-pass filter, the application of SMC is the same as that of the SMC-LPF in Figure 3 except that the low-pass filter is not used.

In all four methods, $T_G = 2$, $T_Q = 1.5$, and $\text{COMRATE}_m = 1.3$. T_G is determined by the handling ability in container ports, and T_Q is different with T_G to compare ufr(∞) among different methods. In TM, SMC, and SMC-LPF, $T_F = 3$, $T_U = 0.5$, and $T_I = 0.5$. In the PSO method, T_G and T_Q are fixed values, while T_F, T_U, and T_I are optimized with ITAE of ufr as the fitness function. The ranges of T_F, T_U, and T_I are [3, 30], [0.1, 7], and (0, 1], respectively. In the SMC-LPF, it is assumed that the handling chain system has reached stability at the initial moment, and $u_1(0_+) = u(0_+)$.

In all cases, the initial values of ufr, arate, and comrate are 1, 0, and 0, respectively. It is expected that unsatisfied freight requirement would reduce to 0 or as small as possible. And then the expected ufr in the calculation of ITAE is set to 0.

4.1. Simulations on Certain HCS. In this section, the handling chain system is certain, and there are no uncertain factors such as parametric perturbation, external disturbances, and other contingencies.

4.1.1. fr Is a Unit Step Signal. In Case 1, fr is a unit step signal, and it can be calculated that

$$\text{avfr} = 1 - \exp\left(\frac{-t}{T_F}\right). \tag{33}$$

And it can be proved that formula (24) is met. The best T_F, T_U, and T_I obtained by the PSO method are $T_F = 6.8120$, $T_U = 0.1$, and $T_I = 0.4313$. The comparisons of ufr, arate, and ITAE are plotted in Figure 4. To facilitate the visualization of the trend of each curve, the curves are not drawn in the same figure. ufr(max) (the maximum value of ufr), asymptotic value, settling time, ufr(25) (the last value of ufr in 25 days), and ITAE(25) (the last value of ITAE in 25 days) of four methods are compared in Table 1. Based on the asymptotic value of ufr and the error value 0.01, the settling time is calculated.

From Figure 4(a), the values of ufr obtained by TM and PSO both increase first and then decrease. ufr(max) obtained by TM is much larger than that obtained by PSO. The values of ufr obtained by SMC and SMC-LPF, which are almost the same, both decrease from the beginning. ufr obtained by four methods gradually reaches their respective asymptotic value. The asymptotic value obtained by PSO is smaller than that obtained by TM, while it is still larger than those obtained by SMC and SMC-LPF.

From Figure 4(b), arate obtained by TM declines from 2 and eventually reaches 1. arate obtained by PSO decreases from 10 to 0, then gradually increases to 1, and finally stabilizes at 1. The values of arate obtained by SMC and SMC-LPF are both 1.3 at the beginning, then decreases to 1, and eventually stabilizes at 1. There is a significant chattering between 2.5 and 5 days in arate obtained by SMC. The chattering has been greatly weakened in arate obtained by the SMC-LPF.

From Figure 4(c), the values of ITAE obtained by TM and PSO have been gradually increasing within 25 days. The growth rate of ITAE obtained by TM is significantly higher than that obtained by PSO. The values of ITAE obtained by SMC and SMC-LPF, which are almost the same, both reach a value less than 10.

From Table 1, ufr(max), asymptotic value, ufr(25), and ITAE(25) obtained by TM are significantly larger than those obtained by other methods. Settling time obtained by TM is shorter than that obtained by PSO, while it is obviously longer than those obtained by SMC and SMC-LPF. All results obtained by PSO are larger than those obtained by SMC and SMC-LPF. ufr(max), asymptotic value, ufr(25), and ITAE(25) obtained by SMC are same or similar to those obtained by the SMC-LPF.

It can be seen that TM and PSO cannot make ufr reach 0 because $T_Q \neq T_G$. It easily results in congestion in container ports in the long term. The asymptotic value obtained by TM is consistent with equation (2), while the asymptotic value obtained by PSO is less than equation (2) because of the nonlinear segments. In SMC and SMC-LPF, ufr can be controlled to reach 0 regardless of whether T_Q and T_G are equal.

In addition, although most results obtained by PSO are better than those of TM, the arate obtained by PSO is too large at the beginning, which would bring great pressure on the handling chain system in container ports. And all results obtained by the SMC-LPF are better than those obtained by TM and PSO, whereas the control effect of SMC is similar to that of the SMC-LPF. The SMC-LPF overcomes the chattering problem of the sliding mode control system for the nonlinear handling chain model in container ports better.

4.1.2. fr Is a Sinusoidal Signal with Offset. In Case 2, fr is a sinusoidal signal with offset. When fr fluctuates as $\text{fr} = (A_1 + A_2 \sin \omega t) \cdot 1(t)$ (to avoid misunderstanding, "(t)" in "$1(t)$" has not been omitted), it can be calculated that

$$\text{FR}(s) = \frac{A_1}{s} + \frac{A_2 \omega}{s^2 + \omega^2}. \tag{34}$$

Then, avfr, the inverse Laplace transform of AVFR(s), is

$$\begin{aligned}\text{avfr} &= L^{-1}\left[\left(\frac{A_1}{s} + \frac{A_2\omega}{s^2+\omega^2}\right)\frac{1}{1+T_F s}\right] \\ &= A_1\left(1 - e^{-t/T_F}\right) + \frac{A_2}{1+T^2\omega^2}\left(-\omega T_F \cos \omega t + \sin \omega t \right. \\ &\quad \left. + \omega T_F \cdot e^{-t/T_F}\right).\end{aligned} \tag{35}$$

It can be proved that formula (24) is met. T_F, T_U, and T_I in the PSO method are the same as those in Section 4.1. The comparisons of ufr, arate, and ITAE are plotted in Figure 5. In order to fully reflect the trends of ufr, arate, and ITAE, each curve is drawn from 0 to 50 days. In the 2nd figure of Figure 5(b), the ordinate of the curve for the first 10 days is

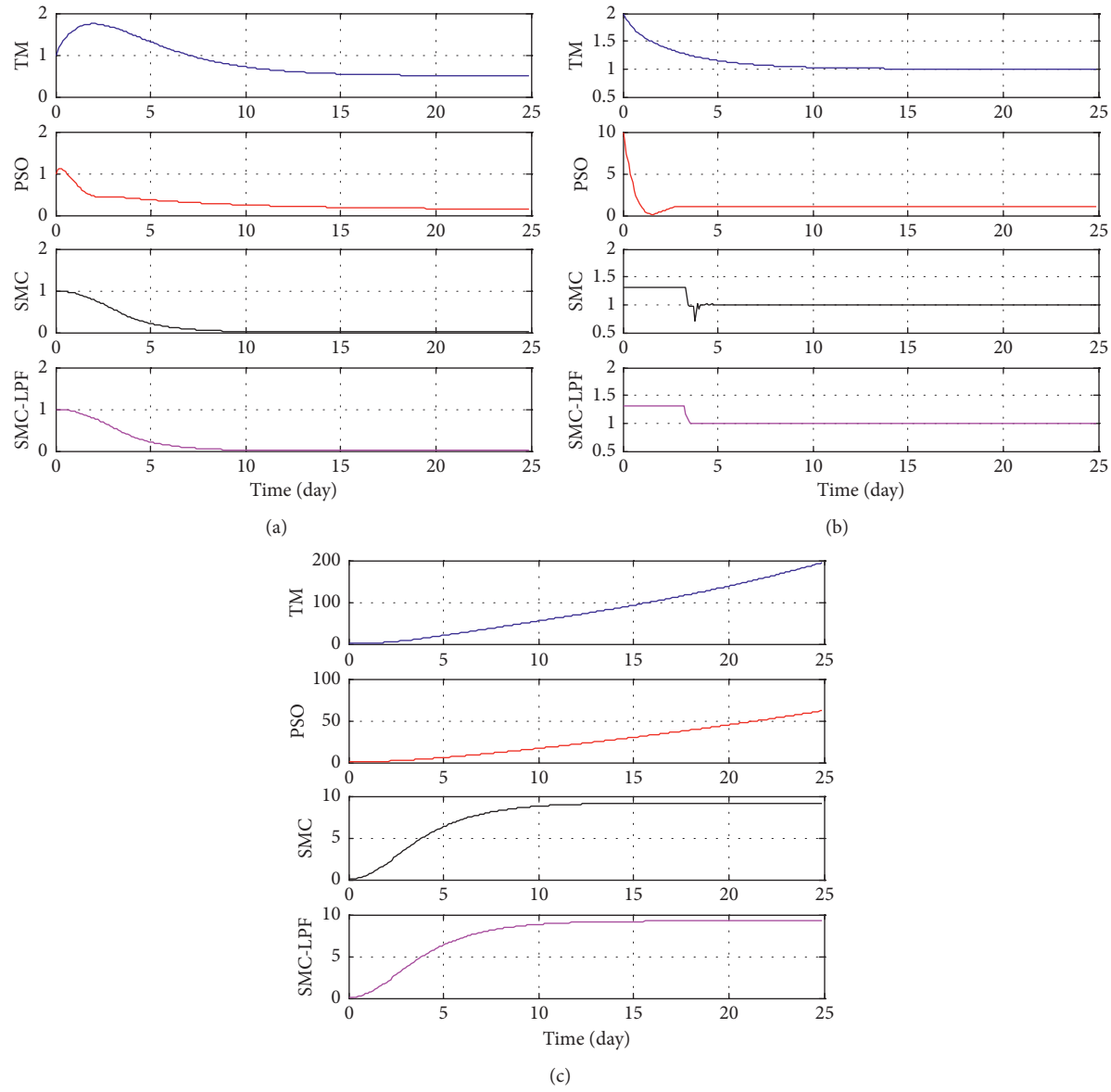

Figure 4: Comparisons of (a) ufr, (b) arate, and (c) ITAE in Case 1.

Table 1: Result comparisons among four methods in Case 1.

Method	ufr(max)	Asymptotic value	Settling time	ufr(25)	ITAE(25)
TM	1.7435	0.5	19.8	0.5018	194.2318
PSO	1.1138	0.1333	26.5	0.1458	61.7083
SMC	1.0000	0	11.2	1.0091×10^{-5}	9.1847
SMC-LPF	1.0000	0	11.3	1.0158×10^{-5}	9.2293

on the left, while the ordinate of the curve for the last 40 days is on the right. The thick dashed line is the dividing line. The ordinate on the left can completely present the initial curve, and the ordinate on the right is consistent with other figures to promote convenient comparison among these figures:

ufr(max), asymptotic value, settling time, ufr(50) (the last value of ufr in 50 days), and ITAE(50) (the last value of ITAE in 50 days) of four methods are compared in Table 2. The values of ufr obtained by TM and PSO are always in flux, so there is no data of asymptotic value and settling time in the rows of TM and PSO.

From Figure 5(a), the values of ufr obtained by TM and PSO both initially increase, then decrease, and finally remain in the flux. The maximum value and the fluctuation of ufr obtained by PSO are much smaller than those of TM. The values of ufr obtained by SMC and SMC-LPF, which are almost the same, both decrease from the beginning and then gradually reach 0.

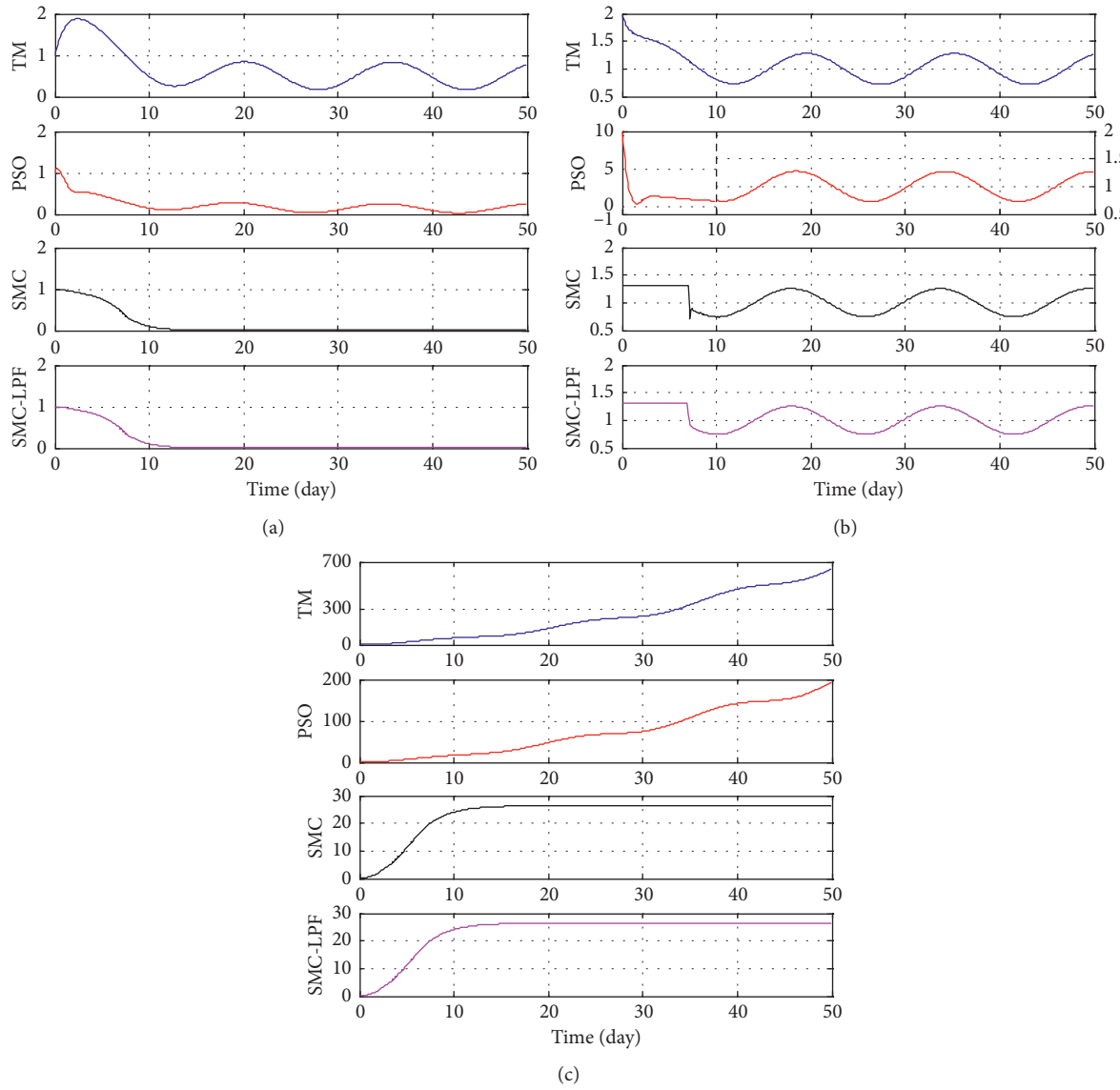

Figure 5: Comparisons of (a) ufr, (b) arate, and (c) ITAE in Case 2.

Table 2: Result comparisons among four methods in Case 2.

Method	ufr(max)	Asymptotic value	Settling time	ufr(50)	ITAE(50)
TM	1.8776	—	—	0.7666	638.3169
PSO	1.1172	—	—	0.2477	192.6649
SMC	1	0	14.8	1.2304×10^{-4}	26.4090
SMC-LPF	1	0	14.8	2.3784×10^{-10}	26.4384

From Figure 5(b), arate obtained by TM begins with a gradual decline from 2 and then has been in volatility. arate obtained by PSO first falls fast from 10 and then continues to fluctuate. arate obtained by SMC and SMC-LPF are both 1.3 at the beginning and then remains in flux. There is little difference among four curves in the fluctuation state between 10 and 50 days. The main difference lies in the variation between 0 and 10 days. Similar to Section 4.1, there is a significant chattering between 5 and 10 days in arate obtained by SMC. The chattering has been greatly weakened in arate obtained by the SMC-LPF.

From Figure 5(c), the values of ITAE obtained by TM and PSO continue to increase within 50 days, although these increases are fluctuating. ITAE obtained by TM is significantly larger than that obtained by PSO. ITAE obtained by SMC and SMC-LPF, which are almost the same, both reach a value less than 30.

From Table 2, ufr(max), ufr(50), and ITAE(50) obtained by SMC are the first largest among four methods. ufr(max), ufr(50), and ITAE(50) obtained by PSO are the second largest among four methods. ufr(max), asymptotic value, and settling time obtained by SMC and SMC-LPF are the same. There is no overshoot in ufr obtained by SMC and SMC-LPF. The differences among ufr(50) and ITAE(50) obtained by SMC and SMC-LPF are very small.

From result comparisons among four methods, PSO can reduce the numerical size and fluctuation of ufr, but it cannot make it close to 0. SMC and SMC-LPF can make ufr reach 0 although $T_Q \neq T_G$ and fr is fluctuating. Similar to those described in Section 4.1, arate obtained by PSO is too large at the beginning, which would bring great pressure on the handling chain system in container ports. arate obtained by SMC and SMC-LPF is between 0 and 1.3, which will not cause this problem brought by PSO. The control effect of the SMC-LPF, which is close to that of SMC, is better than those of TM and PSO. And the chattering problem that exists in SMC is better solved by the SMC-LPF.

4.2. Simulations on Uncertain HCS. Here, parametric (T_G) perturbation, external disturbances, and fluctuant COMRATE$_m$ are discussed in Sections 4.2.1–4.2.3, respectively. To effectively verify the robustness of the proposed method, the values of fr in the following three cases are the same sinusoidal signal with offset as that in Section 4.1.2.

4.2.1. Parametric Perturbation. In Case 3, parametric T_G is not constant, as shown in formula (36), when t is less than 27 days, T_G is equal to 2. When t is in the interval [27, 34), the port's handling ability decreases significantly for some reasons such as equipment failures and operation conflicts, and T_G becomes 14. After active respond, the port's handling ability gradually recoveries. From the 34$^{\text{th}}$ day, T_G is 1.9:

$$T_G = \begin{cases} 2, & t < 27, \\ 14, & 27 \le t < 34, \\ 1.9, & t \ge 34. \end{cases} \tag{36}$$

The comparisons of ufr, arate, and ITAE are plotted in Figure 6. In order to fully display the changes of ufr, arate, and ITAE from the 27$^{\text{th}}$ day when T_G begins to vary, each curve is drawn from the 25$^{\text{th}}$ to 50$^{\text{th}}$ days. To facilitate the identification of chattering in arate, the dotted grid is not drawn in Figure 6(b), and ufr(max), asymptotic value, settling time, ufr(50), and ITAE of four methods are compared in Table 3. Here, we only care about the impact of changes in T_G, the data in the column of "ufr(max)" are the maximum value of ufr from the 25$^{\text{th}}$ to 50$^{\text{th}}$ days, and the data in the column of "ITAE" only calculate the integral of time multiplied by the absolute error for the 27$^{\text{th}}$ to 50$^{\text{th}}$ days. Similar to Table 2, there is no data of asymptotic value and settling time in the rows of TM and PSO because the values of ufr obtained by TM and PSO cannot converge within 50 days.

From Figure 6(a), the values of ufr obtained by TM and PSO still fluctuate during the 27$^{\text{th}}$ to 50$^{\text{th}}$ days. Compared with those in Figure 5(a), they have gradually increased with the increase of T_G. They cannot converge to some asymptotic values in 50 days. The values of ufr obtained by SMC and SMC-LPF begin to increase gradually owing to the change in T_G, reach the peaks around the 36$^{\text{th}}$ day, and then decrease gradually. On the 45$^{\text{th}}$ day or so, they approach 0.

From Figure 6(b), arate obtained by TM has not changed much compared to that in Figure 5(b). This means that TM is not sensitive to the change in T_G. arate obtained by PSO increases significantly from the 28$^{\text{th}}$ day, reaches the maximum value on the 34th day, then gradually decreases, and lastly returns to the original fluctuation state. The values of arate obtained by SMC and SMC-LPF have changed since the 27$^{\text{th}}$ day. They continue to increase after small fluctuations, reach 1.3 on the 31$^{\text{st}}$ day, keep them until the 39$^{\text{th}}$ day, then rapidly decrease, and lastly return to the original fluctuation state. arate obtained by SMC has significant chatters around the 27$^{\text{th}}$ day and 39$^{\text{th}}$ to 41$^{\text{st}}$ days while arate obtained by the SMC-LPF, and these chatters have been significantly weakened.

From Figure 6(c), the values of ITAE obtained by TM and PSO continue to increase especially from the 30$^{\text{th}}$ day, and they are significantly larger than those in Figure 5(c). And ITAE obtained by TM is still much larger than that obtained by PSO. The values of ITAE obtained by SMC and SMC-LPF gradually increase from the original stable value, especially from the 32$^{\text{nd}}$ day; since, about the 44$^{\text{th}}$ day, they have generally reached stability and rarely increased again. There is not much difference between them, which are much smaller than those obtained by TM and PSO.

From Table 3, ufr(max), ufr(50), and ITAE obtained by TM are the first largest among four methods. ufr(max), ufr(50), and ITAE obtained by PSO are the second largest among four methods. Asymptotic values obtained by SMC and SMC-LPF are both 0. ufr(max), settling time, ufr(50), and ITAE obtained by the SMC-LPF are slightly larger than those obtained by SMC.

It can be seen that perturbation in T_G causes significant deterioration in ufr obtained by TM and PSO. However, the parametric perturbation has limited impacts on ufr obtained by SMC and SMC-LPF. SMC and SMC-LPF respond to T_G perturbation more effectively and timely. After limited increases for a short time, the values of ufr obtained by SMC and SMC-LPF are able to converge to 0 again. There is not much difference between results obtained by SMC and SMC-LPF. SMC has the disadvantage of chattering, which has been significantly improved in the SMC-LPF.

4.2.2. External Disturbances. In Case 4, there are external disturbances in this uncertain HCS of container ports, such as bad weather, equipment failure, and traffic congestion. These external disturbances cause fr and comrate' change. After the external disturbances, the freight requirement and container handling completion rate become fr$+f_1$ and comrate'$+f_2$. f_1 and f_2 are

$$\begin{aligned} f_1 &= [f_{10} + A_1 \cdot \sin(\omega_1 t + \varphi_1)] \cdot 1(t - t_1), \\ f_2 &= [f_{20} + A_2 \cdot \sin(\omega_2 t + \varphi_2)] \cdot 1(t - t_2), \end{aligned} \tag{37}$$

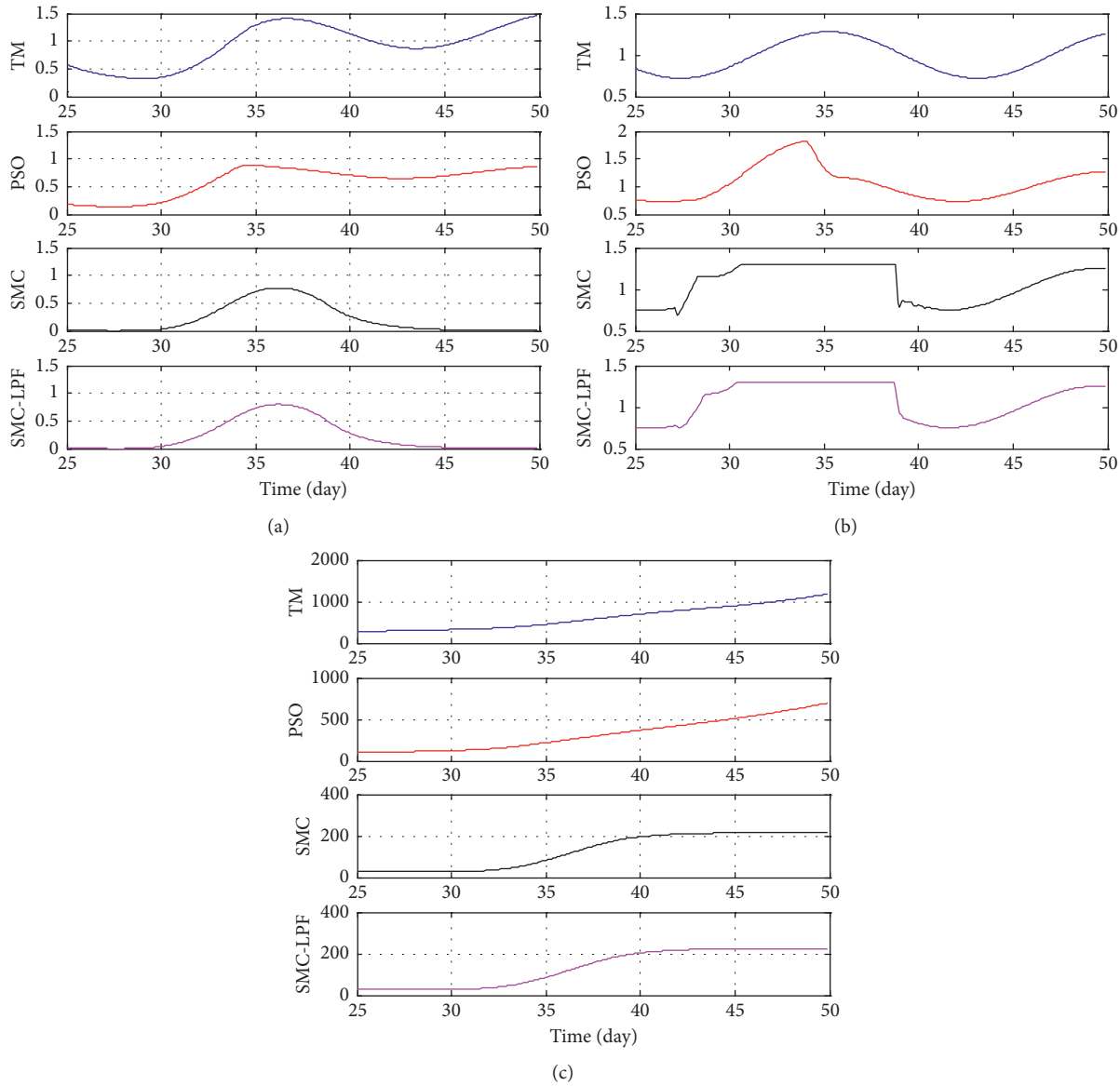

Figure 6: Comparisons of (a) ufr, (b) arate, and (c) ITAE in Case 3.

Table 3: Result comparisons among four methods in Case 3.

Method	ufr(max)	Asymptotic value	Settling time	ufr(50)	ITAE
TM	1.4735	—	—	1.4735	886.4696
PSO	0.8918	—	—	0.8615	586.8973
SMC	0.7720	0	46.6	0.0017	189.2126
SMC-LPF	0.7994	0	46.7	0.0018	198.6476

where $f_{10} = 0.12$, $A_1 = 0.01$, $\omega_1 = 0.5$, $\varphi_1 = 7\pi/12$, $t_1 = 30$, $f_{20} = 0.15$, $A_2 = 0.02$, $\omega_2 = 0.6$, $\varphi_2 = -5\pi/12$, and $t_2 = 40$.

The comparisons of ufr, arate, and ITAE are plotted in Figure 7 ufr(max), asymptotic value, settling time, ufr(60), and ITAE of four methods are compared in Table 4. Due to the occurrence of external disturbances on the 30th day, each curve in Figure 7 is drawn from the 25th to 60th days, data in the column of "ufr(max)" are the maximum value of ufr from the 30th to 60th days, and data in the column of "ITAE" only calculate the integral of time multiplied by the absolute error for the 30th to 60th days.

From Figure 7(a), the values of ufr obtained by TM and PSO both increase significantly from the 30th day, and the values of ufr obtained by SMC and SMC-LPF both increase from the 32nd day. They all peak around the 37th day and then gradually decrease. The peak of ufr obtained by TM is the first largest among four methods. The peak of ufr

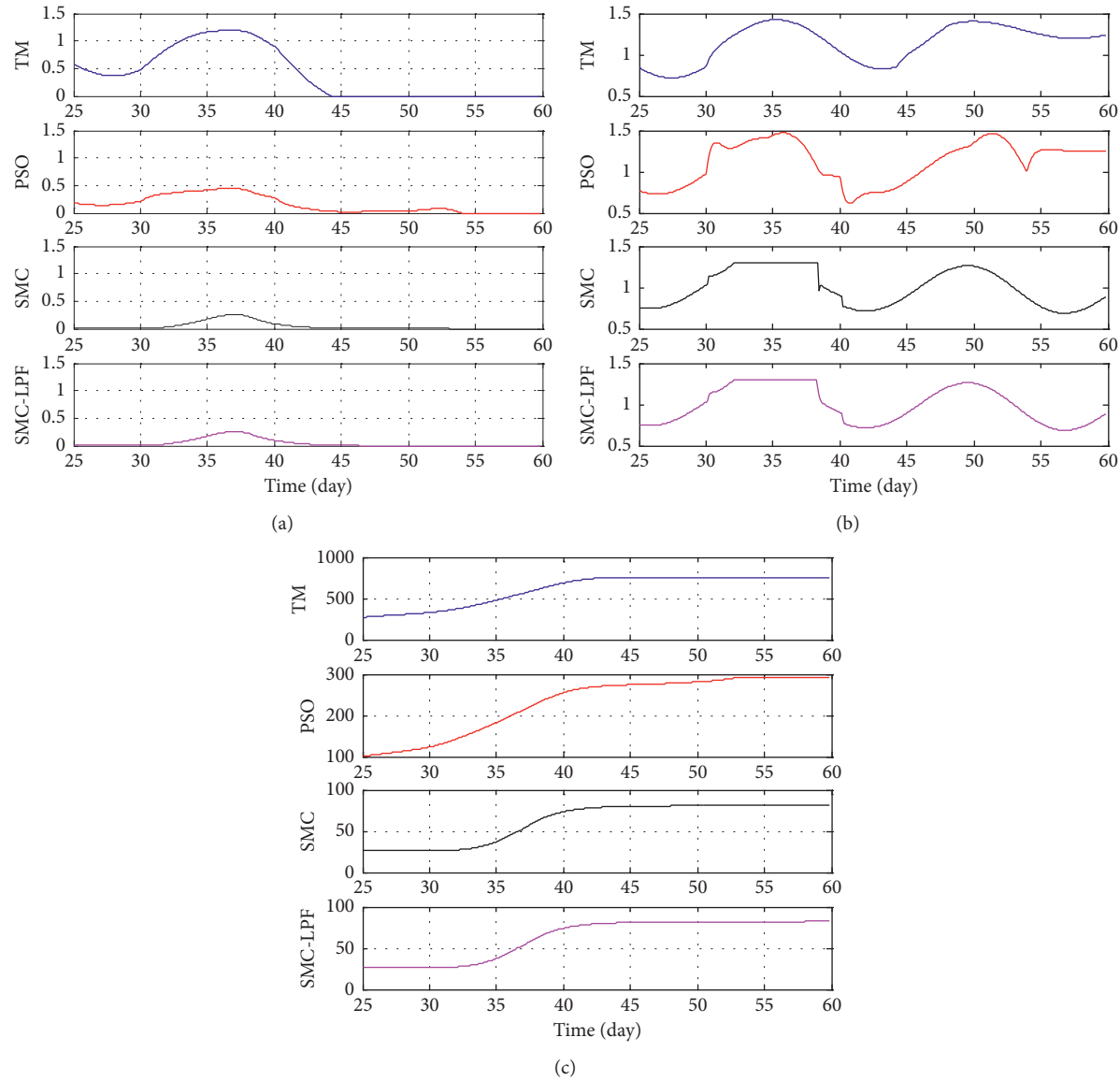

Figure 7: Comparisons of (a) ufr, (b) arate, and (c) ITAE in Case 4.

Table 4: Result comparisons among four methods in Case 4.

Method	ufr(max)	Asymptotic value	Settling time	ufr(60)	ITAE
TM	1.1972	0	44.2	0	426.5556
PSO	0.4492	0	53.9	0	170.2561
SMC	0.2543	0	44.4	0	54.5283
SMC-LPF	0.2549	0	44.1	0	54.6270

obtained by PSO is the second largest among four methods. All ufr obtained by four methods can converge to 0. It is because f_{20} (the average value of f_2 which makes the freight requirement larger) is larger than f_{10} (the average value of f_1 which strengthens port handling ability). Around the 44th day, the values of ufr obtained by TM, SMC, and SMC-LPF have converged to 0. After some slight fluctuations, ufr obtained by PSO does not converge to 0 until the 54th days. The changes of ufr obtained by SMC and SMC-LPF are almost the same.

From Figure 7(b), the values of arate obtained by four methods have significant fluctuations from the 30th day compared with Figure 5(b) arate obtained by PSO fluctuates greatly. The values of arate obtained by TM and PSO have not recovered to their original states within 60 days, while the values of arate obtained by SMC and SMC-LPF have been restored to their original states since 41 days. arate obtained by SMC has significant chattering around the 30th day and the 38th to 41st days, which has been greatly weakened in arate obtained by the SMC-LPF.

From Figure 7(c), the values of ITAE obtained by TM and PSO both continue to increase from the 30th day. ITAE obtained by TM peaks around the 43rd day and then keeps constant, while ITAE obtained by PSO increases until about the 53rd day. The values of ITAE obtained by SMC and SMC-LPF both start to increase from the 32nd to 44th day and then almost keep unchanged. ITAE obtained by TM is much larger than those obtained by other three methods. The difference between ITAE obtained by SMC and SMC-LPF is not obvious, and they are obviously smaller than that obtained by PSO.

From Table 4, ufr(max) and ITAE obtained by TM are the first largest among four methods. ufr(max) and ITAE obtained by PSO are the second largest among four methods. Asymptotic value and ufr(60) obtained by four methods are all 0. There is not much difference among the values of settling time obtained by TM, SMC, and SMC-LPF. Only settling time obtained by PSO is significantly larger than those obtained by other three methods. All results obtained by SMC and SMC-LPF are similar.

It can be seen that external disturbances have obvious impacts on the results obtained by the four methods. The impacts on the results obtained by SMC and SMC-LPF are evidently smaller than those on the results obtained by TM and PSO. The results obtained by SMC and SMC-LPF are not much different. When external disturbances occur, there are obvious chatters in arate obtained by SMC. These chatters in arate can be effectively reduced by the SMC-LPF.

4.2.3. Fluctuant COMRATE$_m$. In Case 5, COMRATE$_m$ is fluctuant in some days. COMRATE$_m$ is

$$\text{COMRATE}_M = \begin{cases} 1.3, & t < 20, \\ 1.15, & 20 \le t < 25, \\ 1.3, & t \ge 25. \end{cases} \tag{38}$$

From formula (38), it can be seen that COMRATE$_m$ has decreased from 1.3 to 1.15 since the 20st day and has not recovered to 1.3 until the 25th day.

The comparisons of ufr, arate, and ITAE are plotted in Figure 8. ufr(max), asymptotic value, settling time, ufr(50), and ITAE of four methods are compared in Table 5. Similar to Section 4.2.1, each curve in Figure 8 is drawn from the 15th to 50th days, data in the column of "ufr(max)" are the maximum value of ufr from the 20th to 50th days, and data in the column of "ITAE" only calculate the integral of time multiplied by the absolute error for the 20th to 50th days. And there is no data of the asymptotic value and settling time in the rows of TM and PSO because the values of ufr obtained by TM and PSO cannot converge within 50 days.

From Figure 8(a), the values of ufr obtained by TM and PSO continue to fluctuate from the 20th day, and they change little compared with Figure 5(a). After the 25th day, they quickly recover to their original fluctuation state. It can be seen that the fluctuation of COMRATE$_m$ in TM and PSO has a small impact on ufr. The values of ufr obtained by SMC and SMC-LPF are always kept at 0. They are completely unaffected by the fluctuation of COMRATE$_m$ in SMC and SMC-LPF.

From Figure 8(b), arate obtained by TM maintains its original fluctuation and does not respond to the change of COMRATE$_m$ in real time. From the 20th to 25th day, arate obtained by PSO experiences a large fluctuation. Around the 20th day, arate obtained by SMC shows a severe chatter and then returns to the original fluctuation state, while arate obtained by the SMC-LPF only changes slightly; at other times, arate obtained by SMC and SMC-LPF are roughly the same.

From Figure 8(c), the values of ITAE obtained by TM and PSO both continue to increase, but obviously the former is much larger than the latter. The values of ITAE obtained by SMC and SMC-LPF are an order of magnitude smaller than that obtained by PSO. After the 25th day, ITAE obtained by SMC increases slightly while that obtained by the SMC-LPF hardly increases.

From Table 5, ufr(max), ufr(50), and ITAE obtained by TM are the largest in those obtained by four methods. ufr(max) and ufr(50) obtained by SMC and SMC-LPF are very close to 0. ITAE obtained by SMC and SMC-LPF are also much smaller than that obtained by PSO. Asymptotic value and settling time obtained by SMC and SMC-LPF are the same with each other. The values of ufr(max) obtained by SMC and SMC-LPF are almost equal. ufr(50) and ITAE obtained by the SMC-LPF are still obviously smaller than those obtained by SMC.

It can be seen that the impact of fluctuant COMRATE$_m$ on results obtained by four methods are not as strong as those in Sections 4.2.1 and 4.2.2. The reason may be COMRATE$_m$ only decreases in a short time and the decrease is small. TM responds less to it. Although the response of PSO is very violent, the control effect is still not as good as SMC and SMC-LPF. To cope with the fluctuation of COMRATE$_m$, arate obtained by SMC generates significant chatter, which is greatly smoothed in arate obtained by the SMC-LPF.

In general, sliding mode control can significantly improve the control effect of the nonlinear handling chain system in container ports and make ufr reach 0 although $T_Q \neq T_G$ and fr is fluctuating. In the cases of parametric (T_G) perturbation, external disturbances, and fluctuant COMRATE$_m$, sliding mode control which can also reduce the impact of these uncertainties on ufr has strong robustness. There exists significant chattering problem in arate obtained by SMC, while the SMC-LPF can effectively overcome the chattering problem. The results of the two cases discussed above show the usefulness of the SMC-LPF, which is highlighted in the analysis. The presented control strategy with little chattering tries to reduce ufr to 0 as close as possible in the nonlinear handling chain system and to maximize the operation resilience. These can be recommended for the partners of port and shipping supply chain to make decisions.

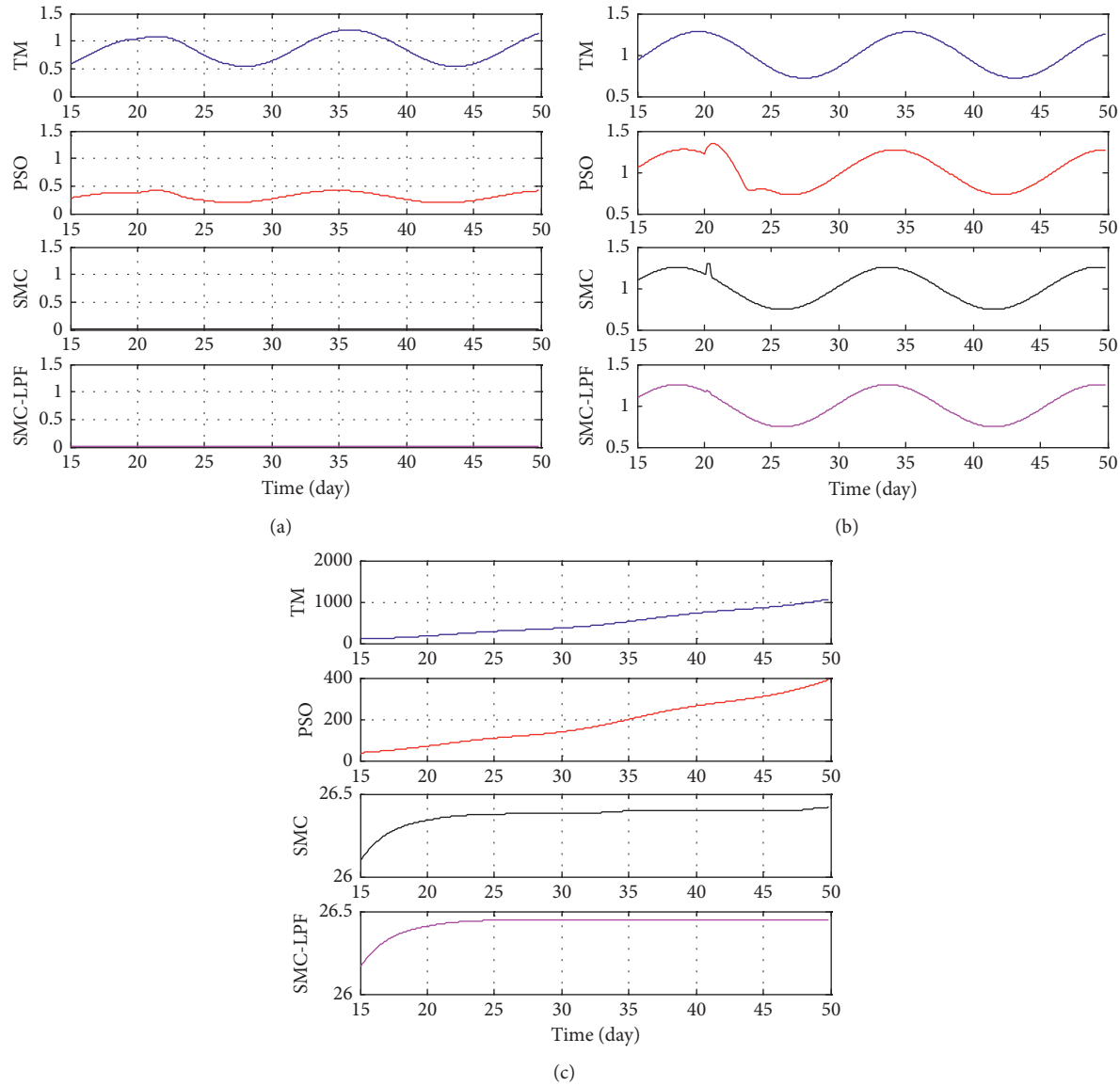

Figure 8: Comparisons of (a) ufr, (b) arate, and (c) ITAE in Case 5.

Table 5: Result comparisons among four methods in Case 5.

Method	ufr(max)	Asymptotic value	Settling time	ufr(50)	ITAE
TM	1.2062	—	—	1.1472	888.4941
PSO	0.4203	—	—	0.4148	320.5332
SMC	$7.8525e-004$	0	14.7	$1.1730e-004$	0.0808
SMC-LPF	$7.5814e-004$	0	14.7	$4.0540e-008$	0.0416

5. Conclusion

This work extends the existing nonlinear model of Xu et al. and explicitly considers the nonnegative unsatisfied freight requirement constraint. Correspondingly, a novel SMC-LPF is designed for the nonlinear handling chain system in container ports. The upper and lower limits of the control signal are well designed to deal with the nonlinear segments. A low-pass filter is added to weaken the chattering problem of sliding mode control. Switching function of sliding mode motion is constructed and the stability of sliding mode motion is analyzed. Exponential reaching law is employed to improve the dynamic quality of the reaching process. The simulation results of fr for a unit step signal and a sinusoidal signal with offset show that the proposed SMC-LPF method can significantly improve the control effect of nonlinear handling chain system in container ports, effectively weaken the chattering problem, and has strong robustness for

uncertainties. Though this work concentrates on container port handling chain system, the proposed framework and method can be applied to the other areas of the port and shipping supply chain.

Data Availability

The data used to support the findings of this study are included within the article.

Conflicts of Interest

The authors declare that they have no conflicts of interest regarding the publication of this article.

Acknowledgments

This work was supported by the National Social Science Foundation Project of China (no. 17CGL018). Here, the authors would like to express their gratitude to it.

References

[1] F. Wang, J. Huang, and Z. Liu, "Port management and operations: emerging research topics and progress," *Journal of Management Sciences in China*, vol. 20, no. 5, pp. 111–126, 2017.

[2] UNCTAD, *50 Years of Review of Maritime Transport, 1968–2018: Reflecting on the Past, Exploring the Future*, UNCTAD, Geneva, Switzerland, 2018, https://unctad.org/en/PublicationsLibrary/dtl2018d1_en.pdf.

[3] J. Xin, R. R. Negenborn, and G. Lodewijks, "Event-driven receding horizon control for energy-efficient container handling," *Control Engineering Practice*, vol. 39, pp. 45–55, 2015.

[4] H. Hu, X. Chen, T. Wang, and Y. Zhang, "A three-stage decomposition method for the joint vehicle dispatching and storage allocation problem in automated container terminals," *Computers & Industrial Engineering*, vol. 129, pp. 90–101, 2019.

[5] B. Xu, J. Li, Y. Yang, H. Wu, and O. Postolache, "Model and resilience analysis for handling chain systems in container ports," *Complexity*, vol. 2019, Article ID 9812651, 12 pages, 2019.

[6] R. Pant, K. Barker, J. E. Ramirez-Marquez, and C. M. Rocco, "Stochastic measures of resilience and their application to container terminals," *Computers & Industrial Engineering*, vol. 70, pp. 183–194, 2014.

[7] A. Mhalla, S. C. Dutilleul, and H. Zhang, "Robust control under uncertainty for seaport handling equipments," *Transportation Research Procedia*, vol. 14, pp. 203–212, 2016.

[8] U. Speer, G. John, and K. Fischer, "Scheduling yard cranes considering crane interference," *Lecture Notes in Computer Science*, vol. 6971, pp. 321–340, 2011.

[9] M. Drexl, "Synchronization in vehicle routing-A survey of VRPs with multiple synchronization constraints," *Transportation Science*, vol. 46, no. 3, pp. 297–316, 2012.

[10] Z.-H. Hu, J.-B. Sheu, and J. X. Luo, "Sequencing twin automated stacking cranes in a block at automated container terminal," *Transportation Research Part C: Emerging Technologies*, vol. 69, pp. 208–227, 2016.

[11] R. Choe, T. S. Kim, T. Kim, and K. R. Ryu, "Crane scheduling for opportunistic remarshaling of containers in an automated stacking yard," *Flexible Services and Manufacturing Journal*, vol. 27, no. 2-3, pp. 331–349, 2015.

[12] S. Li and S. Jia, "The seaport traffic scheduling problem: formulations and a column-row generation algorithm," *Transportation Research Part B: Methodological*, vol. 128, pp. 158–184, 2019.

[13] O. A. Kasm and A. Diabat, "The quay crane scheduling problem with non-crossing and safety clearance constraints: an exact solution approach," *Computers and Operations Research*, vol. 107, pp. 189–199, 2019.

[14] X. F. Yin, L. P. Khoo, and C.-H. Chen, "A distributed agent system for port planning and scheduling," *Advanced Engineering Informatics*, vol. 25, no. 3, pp. 403–412, 2011.

[15] C. Cubillos, R. Díaz, E. Urra, D. Cabrera-Paniagua, G. Cabrera, and G. Lefranc, "An agent-based solution for the berth allocation problem," *International Journal of Computers Communications & Control*, vol. 8, no. 3, pp. 384–394, 2013.

[16] S. Y. Lee and G. S. Cho, "A simulation study for the operations analysis of dynamic planning in container terminals considering RTLS," in *Proceedings of the Second International Conference on Innovative Computing, Information and Control*, pp. 457–460, Kumamoto, Japan, September 2007.

[17] E. Ursavas and S. X. Zhu, "Optimal policies for the berth allocation problem under stochastic nature," *European Journal of Operational Research*, vol. 255, no. 2, pp. 380–387, 2016.

[18] J. Xin, R. R. Negenborn, and G. Lodewijks, "Energy-aware control for automated container terminals using integrated flow shop scheduling and optimal control," *Transportation Research Part C: Emerging Technologies*, vol. 44, pp. 214–230, 2014.

[19] F. B. Boetzelaer, T. J. J. Boom, and R. R. Negenborn, "Model predictive scheduling for container terminals," *IFAC Proceedings*, vol. 47, no. 3, pp. 5091–5096, 2014.

[20] M. A. Dulebenets, "A novel Memetic Algorithm with a deterministic parameter control for efficient berth scheduling at marine container terminals," *Maritime Business Review*, vol. 2, no. 4, pp. 302–330, 2017.

[21] M. A. Dulebenets, M. Kavoosi, O. Abioye, and J. Pasha, "A self-adaptive evolutionary algorithm for the berth scheduling problem: towards efficient parameter control," *Algorithms*, vol. 11, no. 7, pp. 1–35, 2018.

[22] M. Kavoosi, M. A. Dulebenets, O. F. Abioye, J. Pasha, H. Wang, and H. Chi, "An augmented self-adaptive parameter control in evolutionary computation: a case study for the berth scheduling problem," *Advanced Engineering Informatics*, vol. 42, Article ID 100972, 2019.

[23] L. Qiao and W. Zhang, "Double-loop integral terminal sliding mode tracking control for UUVs with adaptive dynamic compensation of uncertainties and disturbances," *IEEE Journal of Oceanic Engineering*, vol. 44, no. 1, pp. 29–53, 2019.

[24] Z. Yan, M. Wang, and J. Xu, "Robust adaptive sliding mode control of underactuated autonomous underwater vehicles with uncertain dynamics," *Ocean Engineering*, vol. 173, pp. 802–809, 2019.